Proceedings of the 8th IEEE Mediterranean Conference
on Control and Automation (MED 2000)
Rio, Patras, GREECE 17-19 July, 2000

Primitive Target Localization and Identification Using CTFM Sonar Imaging

Z. Politis and **P. J. Probert**

University of Oxford, Department of Engineering Science, Robotics Research Group, Parks Road, Oxford OX1 3PJ, UK, zpol,pjp@robots.ox.ac.uk

Abstract. In this paper we introduce a new method for acquiring and processing ultrasound signals for the location and identification of the typical primitives for map building - planes, obtuse angled corners, cylinders, right angled corners and edges. The transducer is a continuous wave single frequency modulated (CFTM) transmitter/receiver, not original in terms of its hardware but with little reported application in this field. Models of the echo signals received allows the feature parametrization of their range and amplitude values with respect to the distance and orientation of the target. Receiver saturation due to the large dynamic range is included in the models. Based on these models and the geometry of a reflection from plane and other targets we proved that only two measurements of the target at two distinctive positions are fulfill the minimum information requirement to localize and classify the studied targets. The proposed method was tested over a set of measurements from the five target types and the results strongly matched the theoretical implications. Applications of this method are suggested.

Keywords. Acoustic sensors, geometrical modeling, CTFM sonar, mobile robots.

1 Introduction

At the first attempts to localize primitive targets scan range and amplitude readings of a single pulse system were used. Their classification never was questioned because planes and right angled corners are unseparable using this short of interpretation. Only edges, whose amplitude was significantly lower, were distinguished. To overcome this problem later attempts introduced pulse systems with multiple receivers, [1]. By using multiple receivers, i.e. taking measurements from different locations, a different interpretation of the environment is obtained in comparison to that of a scan from a stationary position. This alternative representation of the same environment can exploit the geometrical differences between planes and right angled corners. Later studies [2], were based on this idea. In general, the classification of targets has been limited to planes, right angled corners and edges. The reason for this is that the range readings of the sensor can pick up only geometrical differences in the way the reflection is produced. So, primitive targets with the same reflection geometry as the right angled corners, like cylinders, cannot be distinguished.

In this paper a new approach in localization and identification is attempted based on the amplitudes of the reflections. With the use of the CTFM system, where the noise limitations are lower, the amplitude values of the reflections can provide distinctive information about the targets. By using amplitude readings not only we can differentiate planes from corners but we can also classify other types of targets, like edges, obtuse angled corners, and cylinders. In the next section there is a brief presentation of how the CTFM sonar operates and after that the modeling of the primitive targets. In section 4 we will show the difference in the geometry patterns between plane and the rest of the reflectors of reflection from multiple positions followed by a localization and identification method, section 5. In section 6, an ex-

perimental verification of the method is presented.

2 Operation of the CTFM Sonar

The CTFM sonar device is configured with one transmitter and one receiver. A continuous transmission frequency modulated system is used, operating over a frequency range of f_l (45kHz) to f_h (90kHz), using a saw-tooth frequency pattern, better described in [3]. The transmitted signal s_T is of the form

$$s_T(t) = A\mathrm{Re}\left\{e^{2\pi j\left(f_l t_s + \frac{m}{2}t_s^2\right)}\right\} \quad (1)$$

where $t_s = t - t_n$ is the time during a sweep cycle, i.e. $0 \le t_s \le T_s$, $T_s \simeq t_{n+1} - t_n$ (184ms) is the sweep period, and m is a constant ($m = \frac{f_h - f_l}{T_s}$). The time delay between two successive sweeps is ignored.

Assuming a specular reflection with the reflectivity of the surface equals to one, then the signal $s_R(t)$ will be given by integrating over the surface of the transmitter S and the receiver S'

$$s_R(t) = \left| j\frac{s_T(t-\tau)}{\mathcal{J}_T\mathcal{J}_R}\int_S\int_{S'}\frac{e^{j(\omega t - kr)}e^{-\alpha_\lambda r}}{r}dSdS'\right| \quad (2)$$

where $\mathcal{J}_T$ and $\mathcal{J}_R$ are the sensitivities of the transmitter and the receiver (assumed to be constant over the transmitted bandwidth of frequencies), $s_T(t)$ is the transmitted signal, α_λ is the absorption coefficient in the air, r is the distance the wave travels between the elementary surface dS and dS', and k is the wave number. τ is assumed to be constant during the calculation of the integral and is equal to $\tau = \frac{2R}{c}$, where c is the sound velocity and R is distance of the T/R center point to the target.

The double integral includes the attenuation of the signal and the dependence of the received signal on the wavelength λ (which is related with k with $\lambda = \frac{2\pi}{k}$) in the perpendicular direction. We define it as $H(R,\phi,\lambda)$, given by

$$H(R,\phi,\lambda) = \left|\int_S\int_{S'}\frac{e^{-jkr}e^{-\alpha_\lambda r}}{r}dSdS'\right| \quad (3)$$

For simplicity, we assume that

$$H(R,\phi,\lambda) \approx H_r(R,\lambda)H_a(\phi,\lambda) \quad (4)$$

where H_r is the axial response and H_a the angular response of the target.

Mixing the returning signal (s_R) with the one currently being transmitted, and filtering out high frequencies, produces a difference signal, called beat signal, s_a. The amplitude spectrum of the beat signal is the CTFM *sonar image* which corresponds to an one dimensional range map.

3 Target Reflection Modeling

Primitive target modeling has been examined in the past using the pulse system. In [4, 5] a physically based simulation model for the acoustic sensor was introduced for plane, corner, and edge targets. In this paper the extraction of a physical model for various primitive targets is attempted using the CTFM system. The aim of the modeling is to determine the variations at the amplitude of the reflection with respect to the range and orientation.

3.1 Planes

Assume the T/R pair located in front of a plane, displaced by b (0.01m), and of diameter a (0.01m) illustrated in Fig. 1, mounted on a base able to rotate in one direction. The receiver can

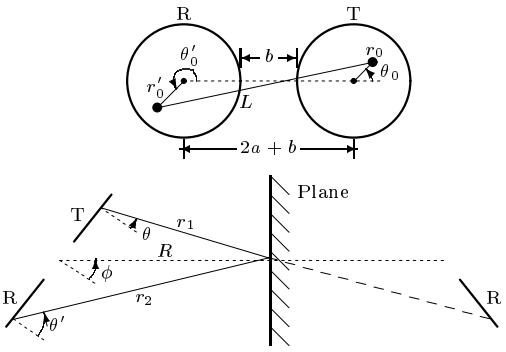

Figure 1: The T/R pair and a reflection from a plane.

be considered as its mirror image on the plane.

Axial and angular response

In the special case where $\phi = 0$, the distance r can be expressed as $r = \sqrt{r_p^2 + L_y^2}$ where r_p is the projected distance r on the azimuth plane and L_y is the relative difference of the distances of dS and dS' from the centers of the transmitter and receiver equal to $L_y = r_0\sin\theta_0 - r_0'\sin\theta_0'$. The distance r_p is given by $r_p = \sqrt{4R^2 + L_x^2 + 4R(L_{x2} - L_{x1})\sin\phi - 4L_{x1}L_{x2}\sin\phi^2}$ where where L_x is the projection of $L = \sqrt{L_x^2 + L_y^2}$ on the azimuth plane and equals to $L_x = L_{x1} + L_{x2}$ with $L_{x1} = a + b/2 + r_0\cos\theta_0$ and $L_{x2} = a + b/2 - r_0'\cos\theta_0'$ and R is the distance of the center of the T/R from the plane. Hence the factor $H_r(R,\lambda)$ is given by

$$H_r(R,\lambda) = \left|\int_S\int_{S'}\frac{e^{-jk\sqrt{r_p^2+L_y^2}}e^{-\alpha_\lambda\sqrt{r_p^2+L_y^2}}}{\sqrt{r_p^2+L_y^2}}dSdS'\right| \quad (5)$$

In the case where the angle ϕ varies, while R is constant and equals to R_0, we assume that the transmitter is a point sourse located in its center and has a directivity diagram N given by $N(\theta,\lambda) = \frac{2\pi a|J_1(ka\sin\theta)|}{ka\sin\theta}$. Then the distance r between the center of T and R is given by $r =$

$\sqrt{4R_0^2 + (2a+b)^2\cos\phi^2}$. If we apply the same to the receiver we get

$$H_a(\phi,\lambda) = N(\theta,\lambda)N(\theta',\lambda) \quad (6)$$

where the angles θ and θ' are related to the angle between the transducer and reflector plane ϕ by

$$\phi = \frac{\theta+\theta'}{2} \quad \text{and} \quad \cos(\phi-\theta) = \frac{2R_0}{r} \quad (7)$$

3.2 Right angled corners

Corners of right angles have exactly the same characteristics as planes, but the angles of incidence at the transmitter and receiver are equal ($\phi = \theta = \theta'$) since r_1 is parallel to r_3, as it can be observed at Fig. 2. In this figure all the distances are projected on the azimuth plane.

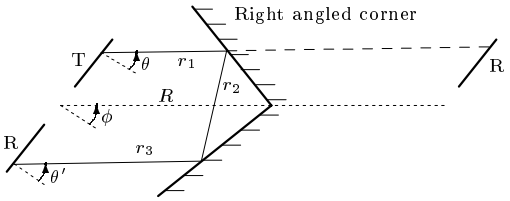

Figure 2: A reflection from a corner.

Axial and angular responses

The expression for $H_r(R,\lambda)$ is the same as in equation 5, where, from the geometry in Fig. 2, $r_p = \sqrt{4R^2 + (L_{x1}-L_{x2})^2}$. L_{x1} and L_{x2} are the projected distances on the azimuth plane between the center of the T/R and dS and dS' respectively and are given by $L_{x1} = a + \frac{b}{2} + r_0\cos\theta_0$ and $L_{x1} = a + \frac{b}{2} - r_0'\cos\theta_0'$.

Similarly the angular response can be determined from the factor H_a

$$H_a(\phi,\lambda) = N(\phi,\lambda)^2 \quad (8)$$

3.3 Cylinders

In the case of a cylinder we assumed that the reflections occur on a vertical line on the surface. The curvature of the cylinder introduces further attenuation of the signal, Fig. 3, given by

$$\rho_{cy} = \frac{\sqrt{\lambda}}{\pi\sqrt{r_2}}\left|\sum_{m=0}^{\infty}\epsilon_m \sin\gamma_m e^{-i\gamma_m}\right| \quad (9)$$

where r_2 is the distance of the reflecting point to the elementary receiver, $\epsilon_0 = 1$ and $\epsilon_m = 2$ and γ_m is an angle given by

$$\gamma_m = ka - \frac{1}{2}\pi(m+\frac{1}{2}), m \geq 0 \quad (10)$$

assuming that $ka \gg m + \frac{1}{2}$.

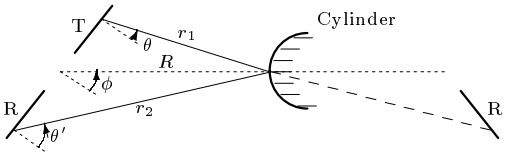

Figure 3: A reflection from a cylinder.

Axial and angular responses

The expression for $H_r(R,\lambda)$ is the same as in equation 7, but the distance r is given by $r = r_1 + r_2$, where $r_1 = \sqrt{R^2 + (\frac{y_0'-y_0}{2})^2 + (x_0 + \frac{2a+b}{2})^2}$ and $r_2 = \sqrt{R^2 + (\frac{y_0'-y_0}{2})^2 + (x_0' + \frac{2a+b}{2})^2}$ with $y_0 = r_0\sin\theta_0$, $y_0' = r_0'\sin\theta_0'$, $x_0 = r_0\cos\theta_0$, and $x_0' = r_0'\cos\theta_0'$. As a result the factor $H_r(R,\lambda)$ will take the following form

$$H_r(R,\lambda) = \left|\int_S\int_{S'}\frac{e^{-jkr}e^{-\alpha_\lambda r}\rho_{cy}dSdS'}{r}\right| \quad (11)$$

The factor $H_a(\phi,\lambda)$ will be the same as in equation 6 with $r_1 = \sqrt{R_0^2 + D^2 - 2R_0D\sin\phi}$ and $r_2 = \sqrt{R_0^2 + D^2 - 2R_0D\sin\phi}$. The relations which connect the angles θ, θ', and ϕ are

$$\cos(\phi-\theta) = \frac{R_0 - D\sin\phi}{r_1}$$

$$\cos(\theta'-\phi) = \frac{R_0 + D\sin\phi}{r_2} \quad (12)$$

where $D = a + \frac{b}{2}$.

3.4 Edges

In edges, all the reflection points are lying on the intersection line of the two planes composing the edge. This introduces an additional spreading at the reflected rays, which is responsible for the further attenuation of the signal by $\frac{\sqrt{\lambda}}{2\pi\sqrt{r_\sigma}}$, where r_σ is the distance from the reflecting point to the elementary receiver.

3.4.1 Axial and angular responses

Now, the factor H_r takes the form

$$H_r(R,\lambda) = \left|\int_S\int_{S'}\frac{e^{-jkr}e^{-\alpha_\lambda r}\sqrt{\lambda}dSdS'}{2\pi r\sqrt{r_2}}\right| \quad (13)$$

where $r = r_1 + r_2$ and r_1 and r_2 are the same as for cylinders. The angular response H_a is the same as for the cylinders.

3.5 Obtuse angled corners

Obtuse angled corners have the characteristic to reflect the emitted rays in such a way that there is no possibility for them to return to the receiver, assuming only reflections at the planes that compose the corner. So, the only reflection that occurs

is that on the intersection semicylindrical alcove of the two planes. As a result, reflections from obtuse angled corners are considered to be very weak, since the radius of the semicylindrical alcove is usually very small.

3.5.1 Axial and angular responses

The distance r is given by $r = r_1 + r_2$, where again r_1 and r_2 are the same as for cylinders, while the the factor $H_r(R, \lambda)$ is expressed as

$$H_r(R,\lambda) = \left| \int_S \int_{S'} \frac{e^{-jkr} e^{-\alpha_\lambda r} \rho_{oc} dS dS'}{r} \right| \quad (14)$$

The factor ρ_{oc} is given from equation 9, but since $ka \ll m + \frac{1}{2}\ \gamma_m$ is now given by

$$\gamma_m = -\frac{\pi m}{(m!)^2} (\frac{ka}{2})^{2m}, m > 0 \quad (15)$$

and $\gamma_0 = \pi(\frac{ka}{2})^2$. For $f = 67.5$kHz, $k = 1234.7$ and $a = 2.8 \cdot 10^{-4}$ we get $\rho_{oc} = \frac{\sqrt{\lambda}}{10\pi\sqrt{r_2}}$ The factor $H_a(\phi, \lambda)$ is given by equation 6. The relations which connect the angles θ, θ', and ϕ are the same as for cylinders, equation 12.

3.6 Amplitude of the reflection with range and bearing

The CTFM sonar image is determined from the beat signal

$$S_a(f) = \frac{KA^2}{4\mathcal{J}_T \mathcal{J}_R} \left(X(f - \frac{2mR}{c}) + X(f + \frac{2mR}{c}) \right) \quad (16)$$

where $X(f)$ is the amplitude of the Fourier transform of $H(R, \phi, \lambda)$. As a consequence, the image includes only a tone spaced at a frequency proportional to the range of the target and modulated by H, defined in the last section for each of the different targets. The beat signal has been sampled at 25kHz and 2048 samples were taken resulting to a resolution of 8.6mm, slightly larger than the 8.2mm resolution of the sonar according to the Rayleigh criterion ($1.6\lambda_\alpha$, where λ_α is the wavelength of the average transmitted frequency).

The maximum amplitude of the Fourier transform of H will determine the amplitude of the tone that appears at the CTFM sonar image, symbolized with $A^t(R, \phi)$, Fig. 4.

There are in practice several sources of inaccuracy which cause errors in applying these ideas, like saturation at close ranges which distorts the amplitude of A^t. To anticipate that, a neural network was trained to model the experimental measurements. At Fig. 5 the modeled axial responses for the studied targets are illustrated. In this plot the obtuse angled corner is of 93°. The right angled corner is a bit higher than the plane due to the additional reflection from the semicylindrical alcove formed at the intersection of the two planes.

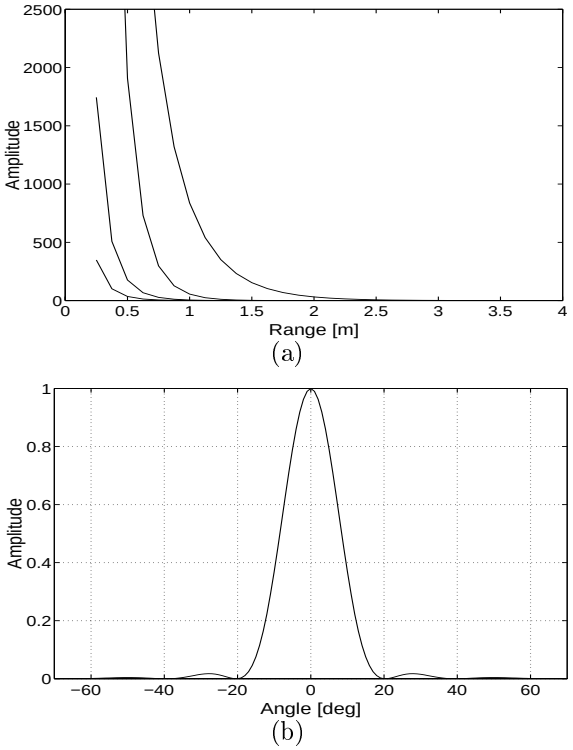

Figure 4: The axial (a) and angular (b) responses in theory. The stronger reflections come from plane and corner targets followed by cylinders (a=0.08m), then by edges and finally by obtuse angled corner (120°).

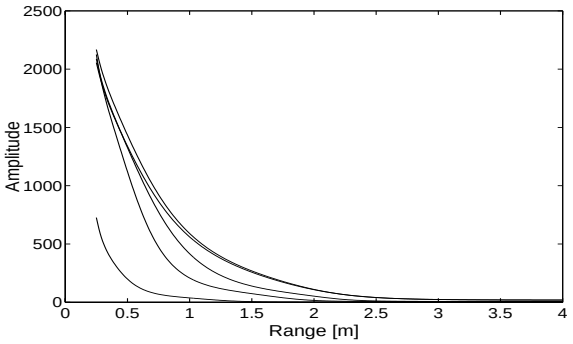

Figure 5: The axial response of the targets modeled using a neural network. Higher at the plot is the right angled corner, then the plane, the obtuse angled corner (93°), the cylinder (a=0.08m), and the edge.

The analysis made in this section can be used to model the axial response of near field reflections from these targets.

4 Reflection geometry

Among the examined targets of the previous section, there is an important difference in the reflected amplitude values when the distance and orientation changes are introduced by displacing the transducer rather than taking a scan of it. Planes are behaving in an entirely different way due to their geometry as it can be observed at Fig. 6. Assume that the position of the sensor has been changed by moving (allowing translation and rotation) from one location to another. Let d be the distance between the two points, and λ_1 and λ_2 the angles between the translation vector

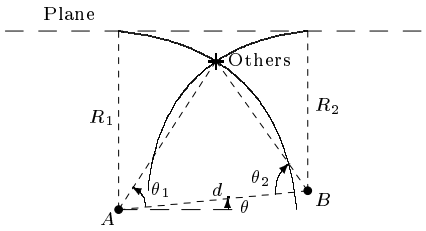

Figure 6: The two possible geometries of reflection from a plane target and any other single point reflective target.

AB and the line of sight of the transducer in the positions A and B respectively. The basic difference among the examined targets is that in case of dispositioning in all the targets the angle between the line of movement of the sensor and the line that connects the target with the sensor is different at the two positions, except from planes. The relation that connects the angle θ between the line of the movement and the plane, and the translation length d is given by

$$R_1 - R_2 = d \sin\theta \tag{17}$$

where R_1 and R_2 are the range of the reflections at the first and second position. The angle θ represents the orientation of the movement of the sensor with respect to the plane target. The angles λ_1 and λ_2 are related with the rotation of the sensor throughout the movement and are supposed to be known. Then the angles ϕ_1 and ϕ_2 between the line of sight and the normal to the target in each position are given by the following equations

$$\phi_1 = \lambda_1 - \theta, \quad \phi_2 = \lambda_2 - \theta \tag{18}$$

So, by measuring the values of R_1 and R_2 we can estimate the orientation of the sensor and the plane target at the two positions, i.e. the values of the angles ϕ_1 and ϕ_2, assuming that the movement of the sensor is known, i.e. the values of d, λ_1 and λ_2.

In case of other targets, if we express the ranges R_1, R_2 and the angles ϕ_1, ϕ_2 of the two reflections as appear at this figure as a function of the distance d between the two positions of the transducer and the angle between the line of movement and the normal to the target line, we get

$$R_1 \cos\theta_1 + R_2 \cos\theta_2 = d, \; R_1 \sin\theta_1 = R_2 \sin\theta_2 \tag{19}$$

Assuming now that the bearing of the sensor with respect to the displacement is known and given by the angles λ_1 and λ_2 at each position, then the equivalent angles ϕ_1 and ϕ_2 between the line of sight and the reflective point of the target can be expressed as

$$\phi_1 = \lambda_1 + \theta_1 - \frac{\pi}{2}, \quad \phi_2 = \lambda_2 + \theta_2 + \frac{\pi}{2} \tag{20}$$

where λ_1 and λ_2 are the angles between the line of sight and the translation line AB of the sensor and are supposed to be known.

In the next section we will show that this alternative modeling of the targets can provide the necessary parameters to localize the target and to discriminate plane and right angled corners or any other of the targets studied before.

5 Localization and identification

The localization of a target is based on estimating the range and the angle between the line-of-sight and the normal of the target. The range is estimated by using the sonar image of one of the two measurements and estimating the frequency of the maximum point of the reflection from the target. The bearing of the target can be estimated by using the range values of the target at the two distinct positions and equation 17 or 19, dependent on the target type. This means that first we have to differentiate the targets into two separate classes according to the geometrical characteristics mentioned in the previous section. To do that we have to interpret the readings of the sonar at the two distinctive positions (these are the range and amplitude of the reflection) according to these models. This means that we have to find a way to estimate which of the two cases our measurements fit better.

Let us first calculate from the measured ranges R_1^e and R_2^e the angles $(\phi_1)_p$ and $(\phi_2)_p$ assuming a plane target and the angles $(\phi_1)_o$ and $(\phi_2)_o$ assuming any other type of target. For both cases, the same pair of the measured amplitude values A_1^e and A_2^e is assumed. Then for each case the values of A_1^e and A_2^e are scaled according to the angular response to get the equivalent amplitude values at the normal direction (i.e. $(\hat{A}_1^e)_p$ and $(\hat{A}_1^e)_o$ at R_1^e and $(\hat{A}_2^e)_p$ and $(\hat{A}_2^e)_o$ at R_2^e).

But the amplitude values of reflections from planes at the normal to the target direction have been modeled with respect to range variations in section 3, Fig. 5. Therefore, the target type can be selected by setting up a criterion to find out the best match of the amplitude values at R_1^e and R_2^e on that plot. A simple and effective way to do that is to choose the target type that produces the minimum outcome for this expression

$$\mathcal{E}_{geom} = \frac{|A_p^t(R_2^e) - \hat{A}_2^e \frac{A_p^t(R_1^e)}{\hat{A}_1^e}|}{A_p^t(R_2^e)} \tag{21}$$

where $A_p^t(\cdot)$ are the expected amplitude values from a plane target. After a decision has been made on the geometry type of the measured target, the bearing angle is equal to $(\phi_1)_p$ and $(\phi_2)_p$ at each position for a plane target, or $(\phi_1)_o$ and $(\phi_2)_o$ respectively for any other target type.

A consequence of the bearing estimation is the classification of the target to planes and other types. In the particular case that the given target is not a plane, we have to further identify what

it is. The only available information are the projected amplitude values $(\hat{A}_1^e)_o$ and $(\hat{A}_2^e)_o$ at the ranges R_1^e and R_1^e respectively. But since the axial response of each target has been modeled, an expression, called $\mathcal{E}_T$, is chosen to measure the fit of the values $(\hat{A}_1^e)_o$ and $(\hat{A}_2^e)_o$ on the curve of the target T at the distances R_1^e and R_1^e

$$\mathcal{E}_T = (A^t(R_2^e) - (\hat{A}_2^e)_o)^2 \qquad (22)$$

The given target is assigned to the target T that minimizes the value of $\mathcal{E}_T$.

6 Experimental verification

Theoretically, we should be able to localize and identify any target of separable axial response. However, in practice it is better to avoid the selection of target types of close amplitude variations with range that may interfere due to the additive noise. The selected targets are a plane, a right angled corner, an edge, a cylinder of 0.08m radius, and an obtuse angled corner of 93°.

Another limitation that will make the identification process even more robust is to assume that the sensor maintain its orientation with respect of the line of movement. This means that the angles of the transducer at each measuring position (λ_1 and λ_2) are equal to each other, and for simplicity equal to zero. A final restriction has to do with the maximum allowed angle between the transducer and the normal direction to the target. If it is very large, i.e. bigger than ±18°, the projection of the amplitude values A_1^e and A_2^e will not be very accurate because the signal to noise ration is very high at these bearing values.

Several pairs of measurements were taken from all the proposed target types to examine the robustness and efficiency of this method. Various ranges were used, in the area of [0.25,3]m, and at various values for the distance d and the angle ϕ resulting to angles ϕ_1 and ϕ_2 always in the region [-18°, 18°]. Fig. 7 shows the estimated positions of the different targets. All of them were recognized successfully. If more than two measurements were taken there would have been an excess of information that could produce more accurate results only on the estimation of the bearing of the target.

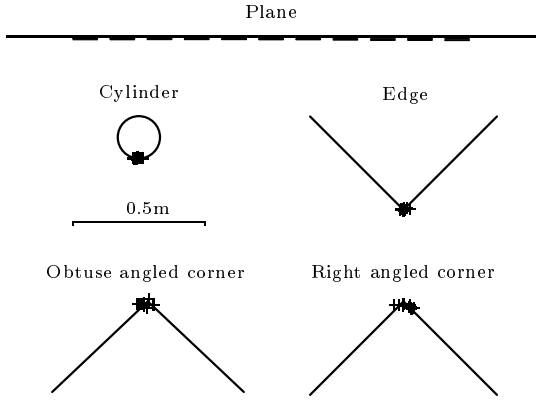

Figure 7: The estimated locations of each target.

7 Conclusions and Discussion

A new method for primitive target localization and identification, using CTFM sonar imaging to interpret the environment, was introduced in this paper. We restricted the environment to single targets to avoid the correspondence problem when multiple reflections from different targets occur. The targets were modeled by exploiting their geometrical characteristics using the properties of acoustic propagation. Then the appropriate features of the model were derived which were based on range and amplitude readings. It is of particular interest that this method requires only two measurements taken from two different positions. In addition it can classify a larger set of primitive targets than the standard one – planes, corners, and edges. Better sensors designed for this application, without saturation problems, will give even more accurate results. These results can be extented to a broader set of specular targets, like semicylindrical alcoves and acute angled corners, to generalize the method even more. This method can be applied for map building or for extracting navigational information for a mobile robot, especially since it is suited for real-time implementations. In addition, CFTM sensor can provide geometrical information about quite complex objects, [6]. Further exploitation could lead to applications in control, inspection and object recognition.

Acknowledgments

One author, Z. Politis, is supported by the State Scholarships Foundation (SSF) of Greece.

References

[1] H. Peremans K. Audenaert and J. M. Van Campenhout. A high-resolution sensor based on tri-aural perception. *IEEE Transactions on Robotics and Automation*, 9(1):36–48, February 1993.

[2] L. Kleeman and R. Kuc. Mobile robot sonar for target localization and classification. *The International Journal of Robotics Research*, 14(4):295–318, August 1995.

[3] Z. Politis and P. Probert. Perception of an indoor robot workspace by using CTFM sonar imaging. *Proceeding of the IEEE International Conference on Robotics and Automation*, May 1998.

[4] R. Kuc and M. W. Siegel. Physically based simulation model for acoustic sensor robot navigation. *IEEE Transactions on Pattern Analysis and Machine Intelligence*, 9(6):766–778, November 1987.

[5] B. Barshan and R. Kuc. Differentiating sonar reflections from corners and planes by employing an intelligent sensor. *IEEE Transactions on Pattern Analysis and Machine Intelligence*, 12(6):560–569, June 1990.

[6] Z. Politis and P. Probert. Modeling and classification of rough surfaces using CTFM sonar imaging. *Proceeding of the IEEE International Conference on Robotics and Automation*, May 1999.